


## Article

# Syntheses, Structures and Properties of Alkali and Alkaline Earth Metal Diamond-Like Compounds $\text{Li}_2\text{MgMSe}_4$ (M = Ge, Sn)

Hongbo Gao <sup>1,2,†</sup> , Kewang Zhang <sup>1,3,†</sup>, Ailijiang Abudurusuli <sup>1,4</sup>, Chen Bai <sup>1</sup>, Zhihua Yang <sup>1</sup>, Kangrong Lai <sup>2</sup>, Junjie Li <sup>1,\*</sup> and Shilie Pan <sup>1,\*</sup>

<sup>1</sup> CAS Key Laboratory of Functional Materials and Devices for Special Environments, Xinjiang Technical Institute of Physics & Chemistry, CAS, Xinjiang Key Laboratory of Electronic Information Materials and Devices, 40-1 South Beijing Road, Urumqi 830011, China; hbgao21@gia.cas.cn (H.G.); zhangkewang@stu.xju.edu.cn (K.Z.); ailijiang18@mails.ucas.ac.cn (A.A.); baichen20@ms.xjb.ac.cn (C.B.); zhyang@ms.xjb.ac.cn (Z.Y.)

<sup>2</sup> Department of Physics, Changji University, Changji 831100, China; laikr0212@cjcu.edu.cn

<sup>3</sup> College of Physical Science and Technology, Xinjiang University, Urumqi 830046, China

<sup>4</sup> Center of Materials Science and Optoelectronics Engineering, University of Chinese Academy of Sciences, Beijing 100049, China

\* Correspondence: lijunjie@ms.xjb.ac.cn (J.L.); slpan@ms.xjb.ac.cn (S.P.)

† These authors contributed equally.



**Citation:** Gao, H.; Zhang, K.; Abudurusuli, A.; Bai, C.; Yang, Z.; Lai, K.; Li, J.; Pan, S. Syntheses, Structures and Properties of Alkali and Alkaline Earth Metal Diamond-Like Compounds  $\text{Li}_2\text{MgMSe}_4$  (M = Ge, Sn). *Materials* **2021**, *14*, 6166. <https://doi.org/10.3390/ma14206166>

Academic Editor: George Wardeh

Received: 31 August 2021

Accepted: 5 October 2021

Published: 18 October 2021

**Publisher's Note:** MDPI stays neutral with regard to jurisdictional claims in published maps and institutional affiliations.



**Copyright:** © 2021 by the authors. Licensee MDPI, Basel, Switzerland. This article is an open access article distributed under the terms and conditions of the Creative Commons Attribution (CC BY) license (<https://creativecommons.org/licenses/by/4.0/>).

**Abstract:** Two new diamond-like (DL) chalcogenides,  $\text{Li}_2\text{MgGeSe}_4$  and  $\text{Li}_2\text{MgSnSe}_4$ , have been successfully synthesized using a conventional high-temperature solid-state method. The two compounds crystallize in the non-centrosymmetric space group  $Pmn2_1$  with  $a = 8.402$  (14) Å,  $b = 7.181$  (12) Å,  $c = 6.728$  (11) Å,  $Z = 2$  for  $\text{Li}_2\text{MgSnSe}_4$ , and  $a = 8.2961$  (7) Å,  $b = 7.0069$  (5) Å,  $c = 6.6116$  (6) Å,  $Z = 2$  for  $\text{Li}_2\text{MgGeSe}_4$ . The calculated results show that the second harmonic generation (SHG) coefficients of  $\text{Li}_2\text{MgSnSe}_4$  ( $d_{33} = 12.19$  pm/v) and  $\text{Li}_2\text{MgGeSe}_4$  ( $d_{33} = -14.77$  pm/v), mainly deriving from the  $[\text{MSe}_4]$  (M = Ge, Sn) tetrahedral units, are close to the one in the benchmark  $\text{AgGaS}_2$  ( $d_{14} = 13.7$  pm/V). The calculated band gaps for  $\text{Li}_2\text{MgSnSe}_4$  and  $\text{Li}_2\text{MgGeSe}_4$  are 2.42 and 2.44 eV, respectively. Moreover, the two compounds are the first series of alkali and alkaline-earth metal DL compounds in the  $\text{I}_2\text{-II-IV-VI}_4$  family, enriching the structural diversity of DL compounds.

**Keywords:** diamond-like structure; chalcogenides; infrared nonlinear optical materials; second harmonic generation

## 1. Introduction

The exploration of advanced functional materials, as well as the development of structural chemistry, depends on the fabrication of new compounds with a special crystal structure, which contains distinctive physical and chemical behaviors [1–12]. A diamond-like (DL) structure compound, exhibiting abundant chemical diversities and adjustable optical properties, has been proven as a valid structural framework for the design and fabrication of new infrared (IR) optical materials, especially for the mid- or far-IR nonlinear optical (NLO) materials. Over the past few decades, a large number of non-centrosymmetric DL chalcogenide compounds, such as  $\text{Li}_4\text{HgGe}_2\text{S}_7$  [13] and  $\text{Li}_4\text{MgGe}_2\text{S}_7$  [14] in the  $\text{I}_4\text{-II-IV}_2\text{-VI}_7$  family, and  $\text{Li}_2\text{CdGeSe}_4$  [15],  $\text{Li}_2\text{CdGeSe}_4$  [16],  $\text{Li}_2\text{ZnGeSe}_4$  [17] and  $\text{Cu}_2\text{ZnSnS}_4$  [18] in the  $\text{I}_2\text{-II-IV-VI}_4$  family, with outstanding optical properties, have been developed using an atomic substitution or co-substitution strategy.

In a DL compound, the cation is coordinated with four anions, and follows the Pauling's electrostatic valency rule [19–23]. Hence, the optical properties including band gap and SHG response in the DL chalcogenide compounds could be effectively regulated by organizing proper tetrahedral units in the structure. On the basis of the statistical

analyses, the DL chalcogenide compounds mainly consisted of univalent metal tetrahedral units, such as alkali metal tetrahedral  $\text{LiQ}_4$  ( $\text{Q} = \text{S}, \text{Se}$ ) and/or IB group metal tetrahedral  $\text{M}^{\text{I}}\text{Q}_4$  ( $\text{M}^{\text{I}} = \text{Cu}, \text{Ag}$ ;  $\text{Q} = \text{S}, \text{Se}$ ), with IIB (Zn, Cd and Hg), IIIA (B, Al, Ga and In), IVA (Si, Ge and Sn) and VA (P and As) group element tetrahedral units [24–27]. Most recently, Pan and Li et al. [14] demonstrated that the alkaline-earth metal  $\text{AQ}_4$  ( $\text{A} = \text{Be}, \text{Mg}$ ;  $\text{Q} = \text{S}, \text{Se}$ ) tetrahedral units, which without  $d-d$  and  $f-f$  electronic transitions, can be used to regulate the optical properties of DL chalcogenide compounds. By introducing alkaline-earth metal tetrahedral unit  $\text{MgS}_4$  into the  $\text{I}_4\text{-II-IV}_2\text{-Q}_7$  system, the first alkali and alkaline-earth metal DL sulfide  $\text{Li}_4\text{MgGe}_2\text{S}_7$  with excellent IR NLO optical performances was discovered. However, owing to the experimental challenges to obtain the four-coordinated alkaline-earth metal  $\text{AQ}_4$  tetrahedral units in a crystal structure, the number of reported alkaline-earth metal containing DL compounds is very limited, and the exploration of new IR NLO materials, especially with excellent optical properties in alkali and alkaline-earth metal DL chalcogenide compounds, is just in the initial stage.

Considering the above discussions, the alkali metal tetrahedral  $\text{LiS}_4$  and alkaline-earth metal tetrahedral  $\text{MgSe}_4$  units were successfully introduced into the classical  $\text{I}_2\text{-II-IV-VI}_4$  family in this work. Two new alkali and alkaline-earth metal DL selenides  $\text{Li}_2\text{MgMSe}_4$  ( $\text{M} = \text{Ge}, \text{Sn}$ ) were synthesized by conventional high temperature solid state reactions in sealed quartz tubes.  $\text{Li}_2\text{MgMSe}_4$  ( $\text{M} = \text{Ge}, \text{Sn}$ ) are isostructural compounds, crystallizing in the orthorhombic  $Pmn2_1$  space group. The compounds exhibit a three dimensional channel structure, which is built by  $[\text{LiSe}_4]$ ,  $[(\text{Li}/\text{Mg})\text{Se}_4]$  and  $[\text{MSe}_4]$  ( $\text{M} = \text{Ge}, \text{Sn}$ ) tetrahedral units. The theoretical investigations show that the calculated band gap for the two compounds is 2.44 eV for  $\text{Li}_2\text{MgGeSe}_4$ , and 2.42 eV for  $\text{Li}_2\text{MgSnSe}_4$  (matched with the experimental value of 2.62 eV). The calculated SHG coefficients of the title compounds are  $d_{33} = 12.19$  pm/V for  $\text{Li}_2\text{MgSnSe}_4$  and  $d_{33} = -14.77$  pm/V for  $\text{Li}_2\text{MgGeSe}_4$ , which are close to the one in  $\text{AgGaS}_2$  ( $d_{14} = 13.7$  pm/V) [28]. The SHG coefficients are mainly contributed by the  $\text{MSe}_4$  ( $\text{M} = \text{Ge}, \text{Sn}$ ) tetrahedral units. Meanwhile, the calculated birefringences are 0.011 for  $\text{Li}_2\text{MgSnSe}_4$  and 0.012 for  $\text{Li}_2\text{MgGeSe}_4$ .

## 2. Experimental Sections

### 2.1. Chemical Syntheses

High purity (99.99%) raw materials (Li, Mg, Sn, Ge and Se) were obtained from Aladdin Industrial Corporation (Fengxian District, Shanghai, China) and utilized without extra purification.

$\text{Li}_2\text{MgMSe}_4$  ( $\text{M} = \text{Ge}, \text{Sn}$ ) single crystals for structural determination were prepared using a melting method in sealed quartz tubes. The starting mixture samples ( $\text{Li}:\text{Mg}:\text{Ge}:\text{Se} = 2:1:1:4$ ;  $\text{Li}:\text{Mg}:\text{Sn}:\text{Se} = 2:1:1:4$ ) were packaged in graphite crucibles in a glove box. After that the graphite crucibles were moved into quartz tubes, and the quartz tubes were sealed by flame under a vacuum atmosphere (about  $10^{-3}$  Pa). Then, the samples were heated to 880 °C in 46 h, and kept at 880 °C for 50 h, then cooled to room temperature in 48 h. Breaking the tubes, the yellow  $\text{Li}_2\text{MgGeSe}_4$  and  $\text{Li}_2\text{MgSnSe}_4$  single crystals were harvested in the graphite crucibles. It is worth mentioning that the two crystals show strong moisture absorptions in air.

The syntheses of  $\text{Li}_2\text{MgMSe}_4$  ( $\text{M} = \text{Ge}, \text{Sn}$ ) powder samples for performance characterization were tried at a higher temperature. The mixtures of Li, Mg, Ge/Sn and Se elements with an atomic stoichiometric ratio were first weighed, ground and sealed in quartz tubes. The sealed samples were slowly heated to 900 °C (in 60 h) in a muffle furnace, and kept at this temperature for 100 h, then cooled to room temperature in 100 h.

### 2.2. Single-Crystal X-ray Diffractions

$\text{Li}_2\text{MgMSe}_4$  ( $\text{M} = \text{Ge}, \text{Sn}$ ) single crystals were manually picked out and utilized for structural determinations. The X-ray diffraction data of  $\text{Li}_2\text{MgMSe}_4$  ( $\text{M} = \text{Ge}, \text{Sn}$ ) single crystals were collected in a Bruker D8 Venture diffractometer that was equipped with monochromatic  $\text{Mo-K}\alpha$  radiation ( $\lambda = 0.71073$  Å) operating at 50 kV and 40 mA. The

structure refinements of the two compounds were carried out in the SHELX-97 crystallography software package. The XPREP program was used for the absorption correction (multiscan), the structures of  $\text{Li}_2\text{MgMSe}_4$  ( $M = \text{Sn, Ge}$ ) were checked by PLATON in case of additional symmetry elements [29–31]. The detailed processes can be found in previous works [9,14,32,33]. It is worth noting that the initial Li/Mg occupation from refinement was 0.53715:0.462850 for  $\text{Li}_2\text{MgSnSe}_4$ , and 0.48933:0.51067 for  $\text{Li}_2\text{MgGeSe}_4$ , which is close to 1:1. To maintain the charge balance in the whole structures, the atomic ratio of Li/Mg in both title compounds was set to 1:1. The crystal data and structural refinements of  $\text{Li}_2\text{MgMSe}_4$  ( $M = \text{Ge, Sn}$ ) are listed in Table 1. Meanwhile, the corresponding atomic coordinates, bond distances and angles, isotropic displacement parameters and atomic parameters are shown in Tables S1–S7. Since  $\text{Li}_2\text{MgGeSe}_4$  deliquesces quickly in air, the data collection for  $\text{Li}_2\text{MgGeSe}_4$  was repeated several times using different single crystals. However, the data integrity of  $\text{Li}_2\text{MgGeSe}_4$  is still lower than  $\text{Li}_2\text{MgSnSe}_4$ .

**Table 1.** Crystal data and structural refinements of  $\text{Li}_2\text{MgSnSe}_4$  and  $\text{Li}_2\text{MgGeSe}_4$ .

Empirical Formula	$\text{Li}_2\text{MgSnSe}_4$	$\text{Li}_2\text{MgGeSe}_4$
Formula weight	472.72 g/mol	426.62 g/mol
Temperature	296.15 K	153 (2) K
Crystal system	Orthorhombic	Orthorhombic
Space group	$Pmm2_1$ (No. 31)	$Pmm2_1$ (No. 31)
Unit cell dimensions	$a = 8.402$ (14) Å $b = 7.181$ (12) Å $c = 6.728$ (11) Å	$a = 8.2961$ (7) Å $b = 7.0069$ (5) Å $c = 6.6116$ (6) Å
Volume	405.9 (12) Å <sup>3</sup>	384.33 (5) Å <sup>3</sup>
Z	2	2
Calculated density	3.867 g/cm <sup>3</sup>	3.686 g/cm <sup>3</sup>
Absorption coefficient	21.047 mm <sup>-1</sup>	22.891 mm <sup>-1</sup>
Goodness-of-fit on $F^2$	0.993	1.110
Final R indices [ $F_o^2 > 2\sigma(F_o^2)$ ] <sup>[a]</sup>	$R_1 = 0.0349$ ; $wR_2 = 0.0750$	$R_1 = 0.0350$ ; $wR_2 = 0.0783$
R indices	$R_1 = 0.0401$ ; $wR_2 = 0.0784$	$R_1 = 0.0413$ ; $wR_2 = 0.0831$
Largest diff. peak and hole	2.08 e·Å <sup>-3</sup> and -0.93 e·Å <sup>-3</sup>	1.55 e·Å <sup>-3</sup> and -2.46 e·Å <sup>-3</sup>

<sup>[a]</sup>  $R_1 = \Sigma||F_o| - |F_c||/\Sigma|F_o|$  and  $wR_2 = [\Sigma w(F_o^2 - F_c^2)^2/\Sigma wF_o^4]^{1/2}$  for  $F_o^2 > 2\sigma(F_o^2)$ .

### 2.3. Powder X-ray Diffraction (PXRD)

The Powder X-ray diffraction (PXRD) pattern of  $\text{Li}_2\text{MgSnSe}_4$  was characterized using a Bruker D2 Phaser diffractometer (Bruker Corporation, Karlsruhe, Germany) under  $\text{Cu-K}\alpha$  radiation ( $\lambda = 1.5418$  Å) with a metal holder. Meanwhile, the experimental XRD pattern of  $\text{Li}_2\text{MgSnSe}_4$  (Figure S1) was recorded from 10 to 70° ( $2\theta$ ) with a scan step width of 0.02°. The experimental and calculated PXRD patterns of  $\text{Li}_2\text{MgSnSe}_4$  are shown in Figure S1. Owing to the experimental challenge in synthesizing and characterizing the moisture-sensitive compounds, impurities such as  $\text{SnSe}_2$  and  $\text{SnSe}$  were observed in the synthesized  $\text{Li}_2\text{MgSnSe}_4$  powder samples. However, based on the XRD patterns, the main phase can be determined to be  $\text{Li}_2\text{MgSnSe}_4$ . Meanwhile, compared with  $\text{Li}_2\text{MgSnSe}_4$ ,  $\text{Li}_2\text{MgGeSe}_4$  powder samples exhibit more serious moisture absorption. It was deliquesced too fast in air (the samples were deliquesced in 1 min at room temperature) to finish the PXRD measurement. GSAS was used to fit and refine the powder diffraction data of  $\text{Li}_2\text{MgSnSe}_4$ . The main phase  $\text{Li}_2\text{MgSnSe}_4$  and impurity phases  $\text{SnSe}$  and  $\text{SnSe}_2$  were refined. A certain peak function was fitted with experimental intensity data, and the values of peaks and structural parameters (including background function, lattice parameters, peak parameters, atomic position, preference orientation, etc.) were constantly adjusted during the fitting process until the difference between calculated intensity and experimental intensity stabilized [34]. The multi-phase Rietveld refinement yielded tiny impurities contents such as  $\text{SnSe}_2$  and  $\text{SnSe}$  (total 9.7%) remaining from the starting materials, and a weight fraction of 90.3% of target  $\text{Li}_2\text{MgSnSe}_4$  (Figure S2). The refined structural parameters are provided in Table S8. The large difference in the refinement can be attributed to the

experimental challenge to obtain long time and high quality PXRD data for the moisture-sensitive  $\text{Li}_2\text{MgSnSe}_4$ . However, the refined results are helpful in judging the purity of the product.

#### 2.4. UV–Vis–NIR Diffuse Reflectance Spectroscopy

The diffuse reflectance spectrum of the synthesized  $\text{Li}_2\text{MgSnSe}_4$  powder samples was characterized using a DUV spectrophotometer (Shimadzu SolidSpec-3700, Shimadzu Corporation, Shanghai, China) at room temperature in air. Based on the reflection spectrum, the corresponding absorption spectrum was obtained using the Kubelka–Munk formula [35,36]. The process was completed in 5–10 min.

#### 2.5. Raman Spectroscopy

The Raman spectrum of  $\text{Li}_2\text{MgSnSe}_4$  was characterized on a single crystal in a LABRAM HR Evolution spectrometer.

The  $\text{Li}_2\text{MgSnSe}_4$  single crystal was firstly placed onto a transparent glass slide. Then, a suitable objective lens was used to select the measured area on the crystal. The maximum power of the used laser beam was about 60 mW with a spot size of  $\sim 35 \mu\text{m}$ .

#### 2.6. Theoretical Calculations

Based on the density functional theory (DFT) and CASTEP program, the plane wave pseudopotential was applied to calculate the electronic structures of  $\text{Li}_2\text{MgMSe}_4$  ( $M = \text{Ge}, \text{Sn}$ ) [37]. Meanwhile, the exchange-correlation effects of the compounds were analyzed by using the generalized gradient approximation (GGA) with the Perdew–Burke–Ernzerhof (PBE) function [38,39]. Under the norm conserving pseudopotentials for wave function expansion, the kinetic energy cutoff of the models was set to 450 eV. Moreover, the Brillouin zone [40] contained  $2 \times 2 \times 2$  Monkhorst-pack k-point sampling [41]. The virtual unit cells were used to process the occupancy [42,43].

### 3. Results and Discussion

#### 3.1. Crystal Structure

As shown in Figure 1a,f, the two compounds are isomorphic structures. Herein,  $\text{Li}_2\text{MgSnSe}_4$  is taken as an example of the structure description.  $\text{Li}_2\text{MgSnSe}_4$  crystallizes in the noncentrosymmetric space group  $Pmn2_1$  with  $a = 8.402$  (14) Å,  $b = 7.181$  (12) Å,  $c = 6.728$  (11) Å and  $Z = 2$ . In the asymmetric unit of  $\text{Li}_2\text{MgSnSe}_4$ , there are two Li, one Mg, one Sn and three Se atoms that are crystallographically independent. In  $\text{Li}_2\text{MgSnSe}_4$ , the Li2 and Sn1 atoms are bonded to four Se atoms to build up the  $[\text{LiSe}_4]$  and  $[\text{SnSe}_4]$  tetrahedra with Li–Se bond lengths ranging from 2.50 Å–2.65 Å and Sn–Se bond lengths ranging from 2.505 Å–2.528 Å, respectively. The Li1 and Mg1 atoms are set to share the same sites with the atomic ratio of 1:1 in the initial refinements with the identical anisotropic displacement parameters, which can help to obtain better R values and reasonable temperature factors, similar to the situation of Cu/Mg atomic co-occupation in  $\text{Cu}_2\text{MgSiS}_4$  [44],  $\text{Cu}_2\text{MgGeS}_4$  [44] and  $\text{Cu}_2\text{MgSiSe}_4$  [44]. Furthermore, Li/Mg atomic co-occupation is very common, which can be found in the  $\text{LiMg}(\text{IO}_3)_3$  [45] and  $\text{Li}_{0.8}\text{Mg}_{2.1}\text{B}_2\text{O}_5\text{F}$  [46]. Similar to the Li2 and Sn1 atoms, the co-occupied Li1 and Mg1 atoms are bonded to four Se atoms to construct the  $[(\text{Li}/\text{Mg})\text{Se}_4]$  tetrahedra units at the Wyckoff position 4b (Table S7). Furthermore, the formed tetrahedra groups are connected with each other by sharing Se atoms to constitute the final DL structure. For both compounds, there is a similar channel-like structure with a channel diameter of about 6 Ångstrom on the  $ab$  plane, as shown in Figure 1e,j. On the basis of the detailed investigations in the Inorganic Crystal Structure Database (ICSD), the two compounds should be the first series of alkali and alkaline earth metal DL compounds in the  $\text{I}_2\text{-II-IV-VI}_4$  family.

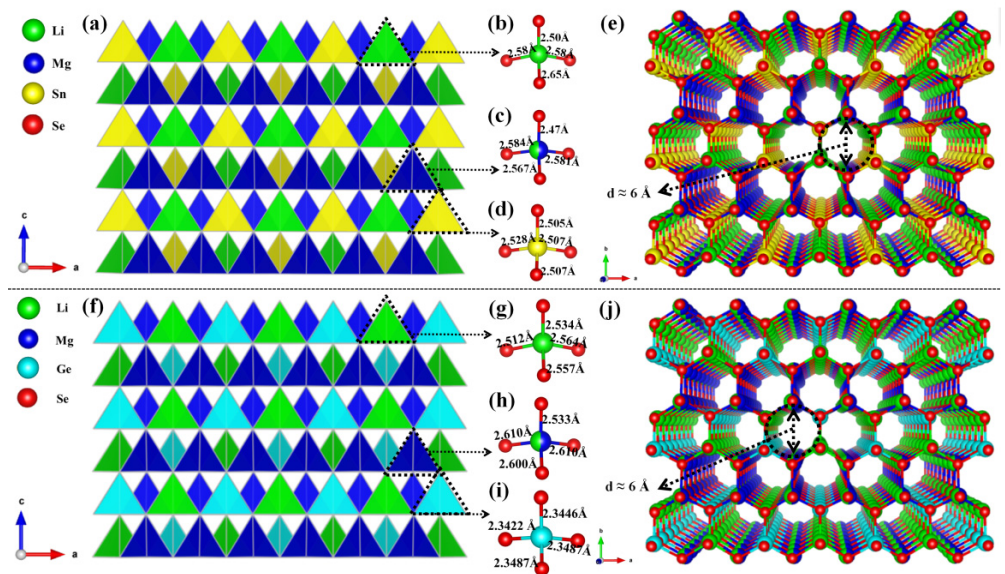


**Figure 1.** The DL structure of  $\text{Li}_2\text{MgSnSe}_4$  (a) and  $\text{Li}_2\text{MgGeSe}_4$  (f) on the  $ac$  plane; (b–d,g–i) The structures of  $[\text{LiSe}_4]$ ,  $[(\text{Li}/\text{Mg})\text{Se}_4]$ ,  $[\text{SnSe}_4]$  and  $[\text{GeSe}_4]$  tetrahedral units. The channel-like structures of  $\text{Li}_2\text{MgSnSe}_4$  (e) and  $\text{Li}_2\text{MgGeSe}_4$  (j) on  $ab$  plane.

### 3.2. Optical Properties

Based on the UV–Vis–NIR diffuse-reflectance spectrum, the experimental band gap of  $\text{Li}_2\text{MgSnSe}_4$  was determined to be 2.62 eV (Figure 2a). To confirm chemical bonding, the Raman spectrum of  $\text{Li}_2\text{MgSnSe}_4$  was characterized on a single crystal. As shown in Figure 2b, the peaks below  $193\text{ cm}^{-1}$  are related to the vibrations of Li–Se and Mg–Se bonding, matched with the previous results [47–49]. The peak at  $193\text{ cm}^{-1}$  and the overlapping peaks around  $235\text{ cm}^{-1}$  could be assigned to the asymmetric and symmetric stretching vibrations of Sn–Se bonding in  $\text{SnSe}_4$  tetrahedral groups [49,50].

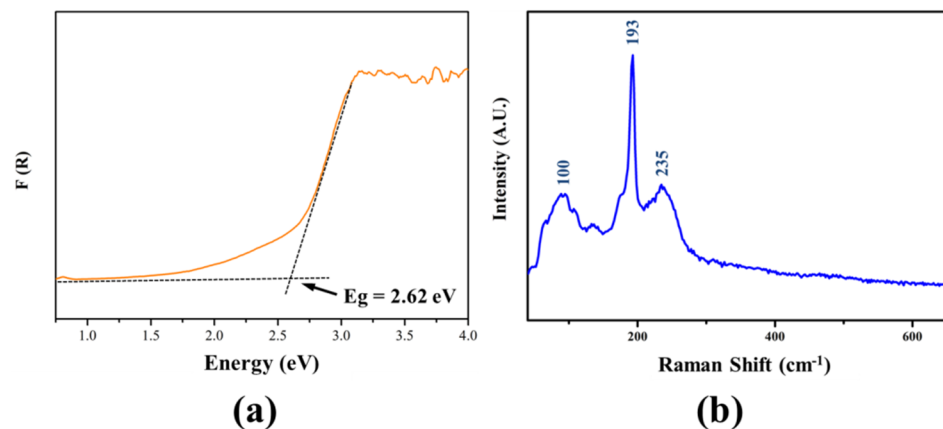


**Figure 2.** (a) Experimental band gap of  $\text{Li}_2\text{MgSnSe}_4$  samples; and (b) Raman spectrum of  $\text{Li}_2\text{MgSnSe}_4$  single crystal.

### 3.3. Theoretical Calculations

To study the linear and nonlinear optical properties of  $\text{Li}_2\text{MgMSe}_4$  ( $M = \text{Ge}, \text{Sn}$ ), DFT calculations were implemented. Considering the Li/Mg atomic co-occupation at the Wyckoff position 4b in the structures, the virtual unit cells were built for the calculations, as shown in Table S9 and Figure S3. The calculated theoretical band gaps, SHG coefficients and birefringences of the two compounds are shown in Table 2; the calculated band gap for the two compounds is 2.44 eV for  $\text{Li}_2\text{MgGeSe}_4$ , and 2.42 eV for  $\text{Li}_2\text{MgSnSe}_4$  (matched with

the experimental value of 2.62 eV). The SHG coefficients of  $\text{Li}_2\text{MgSnSe}_4$  in  $d_{33} = 12.19$  pm/v and  $\text{Li}_2\text{MgGeSe}_4$  in  $d_{33} = -14.77$  pm/v are close to the one of  $\text{AgGaS}_2$  in  $d_{14} = 13.7$  pm/v. The calculated birefringences for the two compounds are 0.011 ( $\text{Li}_2\text{MgSnSe}_4$ ) and 0.012 ( $\text{Li}_2\text{MgGeSe}_4$ ), respectively.

**Table 2.** Calculated band gaps, SHG coefficients and birefringence of  $\text{Li}_2\text{MgSnSe}_4$  and  $\text{Li}_2\text{MgGeSe}_4$ .

Compound	$E_g$ (cal./eV)	$d_{15}$ (pm/v)	$d_{24}$ (pm/v)	$d_{33}$ (pm/v)	$\Delta n@1064$ nm
$\text{Li}_2\text{MgSnSe}_4$	2.42	−4.68	−5.81	12.19	0.011
$\text{Li}_2\text{MgGeSe}_4$	2.4	5.53	7.14	−14.77	0.012

To detect the origin of the optical properties, the electronic structures, SHG densities and band-resolved NLO susceptibilities of  $\text{Li}_2\text{MgMSe}_4$  ( $M = \text{Ge, Sn}$ ) were further investigated. Figure 3 shows the calculated band structures, total and partial density of states and the band-resolved NLO susceptibility  $\chi^{(2)}$  of the two compounds. The band structures (Figure 3a,b) indicate that  $\text{Li}_2\text{MgGeSe}_4$  is an indirect band gap compound with a band gap of 2.44 eV, while  $\text{Li}_2\text{MgSnSe}_4$  is a direct band gap compound with a band gap of 2.42 eV (matched with the experimental value of 2.62 eV). Furthermore, as shown from the total and partial density of states (PDOS) curves (Figure 3c,d), the valence bands maximum (VBM), which, around the Fermi level, is mainly occupied by Se-4p (83%) orbitals with the minor contribution of Sn-5p (8%), Li/Mg-2p (5%) and Li-2s (4%) orbitals for  $\text{Li}_2\text{MgSnSe}_4$  and Se-4p (83%) orbitals with the minor contribution of Ge-4p (8%), Li/Mg-2p (5%) and Li-2s (4%) orbitals for  $\text{Li}_2\text{MgGeSe}_4$ , respectively (the range from −4.0 to 0 eV). The conduction bands minimum (CBM) originates from Se-4p (10%), Sn-5p (9%), Li-2s (19%) and Li/Mg-2p (21%) orbitals for  $\text{Li}_2\text{MgSnSe}_4$ , Se-4p (11%), Ge-4p (8%), Li-2s (17%) and Li/Mg-2p (21%) orbitals for  $\text{Li}_2\text{MgGeSe}_4$ , respectively (the range from 2.4 to 12 eV). The results indicate that the optical band gaps of  $\text{Li}_2\text{MgMSe}_4$  ( $M = \text{Ge, Sn}$ ) are mainly determined by the Se-4p, Li/Mg-2p and Li-2s orbitals.

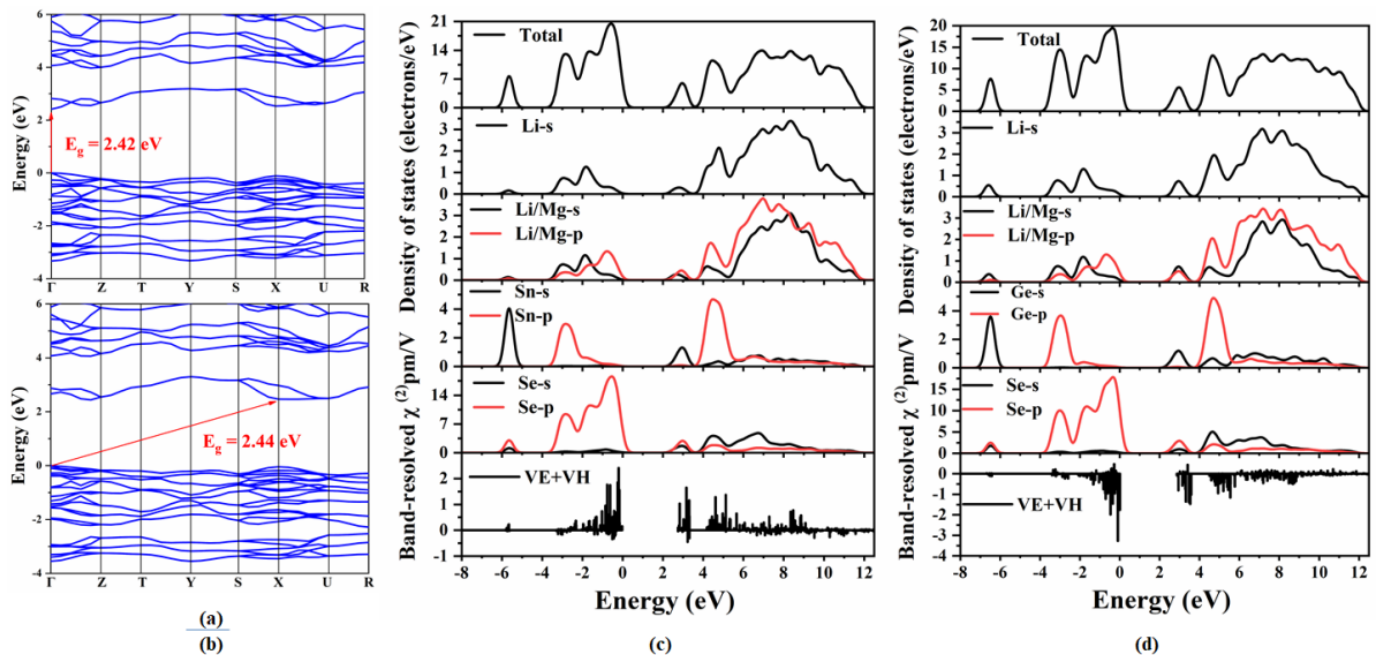


**Figure 3.** Calculated band structures of (a)  $\text{Li}_2\text{MgSnSe}_4$  and (b)  $\text{Li}_2\text{MgGeSe}_4$ ; total and partial density of states and the band-resolved NLO susceptibility  $\chi^{(2)}$  of (c)  $\text{Li}_2\text{MgSnSe}_4$  and (d)  $\text{Li}_2\text{MgGeSe}_4$ .

Figure 4 shows the calculated SHG densities for the two compounds. Combined with the band-resolved NLO susceptibility  $\chi^{(2)}$  in Figure 3c–d, the SHG responses of  $\text{Li}_2\text{MgMSe}_4$

(M = Ge, Sn) can be mainly derived from the  $[MSe_4]$  (M = Ge, Sn) tetrahedra units and with minor contributions from  $[LiSe_4]$  and  $[(Li/Mg)Se_4]$  groups.

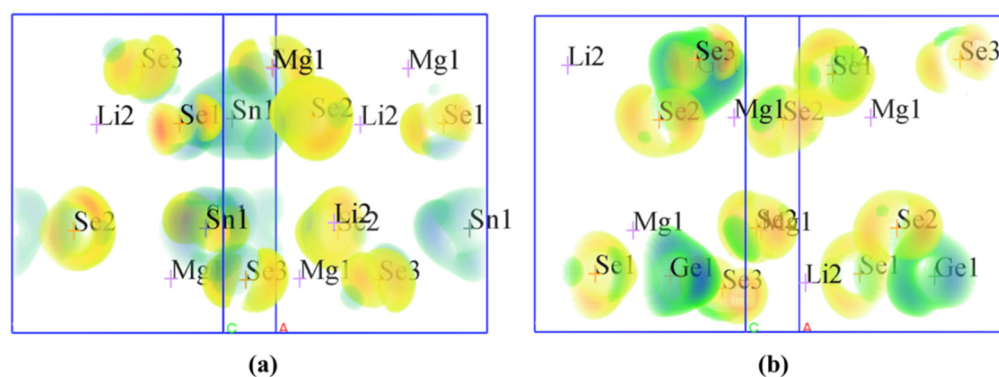


**Figure 4.** SHG densities of (a)  $Li_2MgSnSe_4$  and (b)  $Li_2MgGeSe_4$ .

#### 4. Conclusions

In summary, the first series of DL selenides in the  $I_2-II-IV-VI_4$  family,  $Li_2MgGeSe_4$  and  $Li_2MgSnSe_4$ , have been rationally designed and synthesized. Their crystal structures were determined using single crystal X-ray diffractions, and the optical properties were studied using experimental spectra and DFT calculations.  $Li_2MgMSe_4$  (M = Ge, Sn) crystallize in the non-centrosymmetric space group  $Pmn2_1$  and show channel structures built by  $[LiSe_4]$ ,  $[(Li/Mg)Se_4]$  and  $[MSe_4]$  (M = Ge, Sn) tetrahedra units. The two compounds exhibit large theoretical SHG coefficients in  $d_{33}$  (12.19 pm/v for  $Li_2MgSnSe_4$ , and  $-14.77$  pm/v for  $Li_2MgGeSe_4$ ), moderate band gaps (2.42 for  $Li_2MgSnSe_4$ , and 2.44 for  $Li_2MgGeSe_4$ ) in selenides. The results demonstrated that introducing alkali metal and alkaline earth metal tetrahedral units into the  $I_2-II-IV-VI_4$  family is a feasible way for the development of diamond-like IR nonlinear optical materials with good properties.

**Supplementary Materials:** The following are available online at <https://www.mdpi.com/article/10.3390/ma14206166/s1>, Table S1: Atomic coordinates and equivalent isotropic displacement parameters of  $Li_2MgSnSe_4$ , Table S2: Anisotropic displacement parameters ( $\text{\AA}^2 \times 10^3$ ) of  $Li_2MgSnSe_4$ , Table S3: Symmetry, selected bond lengths and angles of crystal data and structural refinements of  $Li_2MgSnSe_4$ , Table S4: Atomic coordinates and equivalent isotropic displacement parameters of  $Li_2MgGeSe_4$ , Table S5: Anisotropic displacement parameters ( $\text{\AA}^2 \times 10^3$ ) of  $Li_2MgGeSe_4$ , Table S6: Symmetry, selected bond lengths and angles of crystal data and structural refinements of  $Li_2MgGeSe_4$ , Table S7: Atomic parameters of  $Li_2MgSnSe_4$  and  $Li_2MgGeSe_4$ , Table S8: The refined structural parameters of  $Li_2MgSnSe_4$ , Table S9: The crystallographic data of  $Li_2MgMSe_4$  (M = Sn, Ge), Figure S1: Experimental and calculated PXRD patterns of  $Li_2MgSnSe_4$ , Figure S2: The PXRD Rietveld refinement of the obtained  $Li_2MgSnSe_4$  samples, Figure S3: The atomic models of (a)  $Li_2MgSnSe_4$  and (b)  $Li_2MgGeSe_4$ .

**Author Contributions:** H.G. synthesized the crystals, tested the samples, and wrote the manuscript. K.Z. and Z.Y. performed the electronic structure and optical property calculations. A.A. provided the support for the syntheses and structure determination of crystals. C.B. and J.L. provided comments on the revision of the manuscript. J.L., K.L. and S.P. designed and supervised the study. All authors have read and agreed to the published version of the manuscript.

**Funding:** This research was funded by Tianshan Cedar Program (2019XS24), the High-level Talent Project of Xinjiang Uygur Autonomous Region (2020000039), Partnership and International Cooperation Program of Shanghai Cooperation Organization (2020E01040), West Light Foundation of the Chinese Academy of Sciences (2019-YDYLT002), National Natural Science Foundation of China (52002398).

**Data Availability Statement:** The data presented in this study are available in Supplementary Material. The X-ray crystallographic coordinates for structures reported in this study have been deposited at the Cambridge Crystallographic Data Centre (CCDC), under deposition numbers

2106592-2106593. These data can be obtained free of charge from The Cambridge Crystallographic Data Centre via [www.ccdc.cam.ac.uk/datarequest/cif](http://www.ccdc.cam.ac.uk/datarequest/cif) (accessed on 5 October 2021).

**Conflicts of Interest:** The authors declare no conflict of interest.

## References

1. Geng, L.; Meng, C.; Lu, H.; Luo, Z.; Lin, C.; Cheng, W. Bi<sub>2</sub>Te(IO<sub>3</sub>)O<sub>5</sub>Cl: A novel polar iodate oxychloride exhibiting a second-order nonlinear optical response. *Dalton Trans.* **2015**, *44*, 2469–2475. [[CrossRef](#)]
2. Lu, X.; Chen, Z.; Shi, X.; Jing, Q.; Lee, M. Two Pyrophosphates with Large Birefringences and Second-Harmonic Responses as Ultraviolet Nonlinear Optical Materials. *Angew. Chem. Int. Ed.* **2020**, *59*, 17648–17656. [[CrossRef](#)]
3. Liang, F.; Kang, L.; Lin, Z.; Wu, Y. Mid-Infrared Nonlinear Optical Materials Based on Metal Chalcogenides: Structure–Property Relationship. *Cryst. Growth Des.* **2017**, *17*, 2254–2289. [[CrossRef](#)]
4. Kotb, H.; Khater, H.; Saber, O.; Ahmad, M. Sintering Temperature, Frequency, and Temperature Dependent Dielectric Properties of Na<sub>0.5</sub>Sm<sub>0.5</sub>Cu<sub>3</sub>Ti<sub>4</sub>O<sub>12</sub> Ceramics. *Materials* **2021**, *14*, 4805. [[CrossRef](#)] [[PubMed](#)]
5. Rong, L.; Xu, Z.; Sun, J.; Guo, G. New methyl formate synthesis method: Coal to methyl formate. *J. Energy Chem.* **2018**, *27*, 238–242. [[CrossRef](#)]
6. Wu, C.; Yang, G.; Humphrey, M.G.; Zhang, C. Recent Advances in Ultraviolet and Deep-Ultraviolet Second-Order Non-linear Optical Crystals. *Coord. Chem. Rev.* **2018**, *375*, 459–488. [[CrossRef](#)]
7. Mutailipu, M.; Zhang, M.; Zhang, B.B.; Wang, L.Y.; Yang, Z.H.; Zhou, X.; Pan, S.L. SrB<sub>5</sub>O<sub>7</sub>F<sub>3</sub> Functionalized with [B<sub>5</sub>O<sub>9</sub>F<sub>3</sub>]<sup>6−</sup> Chromophores: Accelerating the Rational Design of Deep-Ultraviolet Nonlinear Optical Materials. *Angew. Chem. Int. Ed.* **2018**, *57*, 6095–6099. [[CrossRef](#)]
8. Wang, Y.; Zhang, B.; Yang, Z.; Pan, S. Cation-Tuned Synthesis of Fluorooxoborates: Towards Optimal Deep-Ultraviolet Nonlinear Optical Materials. *Angew. Chem. Int. Ed.* **2018**, *57*, 2150–2154. [[CrossRef](#)]
9. Huang, Y.; Gao, L.; Yu, H.; Yang, Z.; Li, J.; Pan, S. Na<sub>6</sub>MQ<sub>4</sub> (M = Zn, Cd; Q = S, Se): Promising New Ternary Infrared Nonlinear Optical Materials. *Chem. Eur. J.* **2021**, *27*, 6538–6544. [[CrossRef](#)]
10. Xu, F.; Peng, G.; Lin, C.; Zhao, D.; Li, B.-X.; Zhang, G.; Yang, S.; Ye, N. Na<sub>3</sub>Sc<sub>2</sub>(PO<sub>4</sub>)<sub>2</sub>F<sub>3</sub>: Rational design and synthesis of an alkali rare-earth phosphate fluoride as an ultraviolet nonlinear optical crystal with an enlarged birefringence. *J. Mater. Chem. C* **2020**, *8*, 4965–4972. [[CrossRef](#)]
11. Lee, H.; Ok, K.M. Na<sub>2</sub>Mg<sub>1−x</sub>Zn<sub>x</sub>SiO<sub>4</sub> (0 ≤ x ≤ 1): Noncentrosymmetric Sodium Metal Silicate Solid Solutions with Ultraviolet Nonlinear Optical Properties. *Bull. Korean Chem. Soc.* **2020**, *41*, 139–142. [[CrossRef](#)]
12. Kee, J.; Ok, K.M. Hydrogen-Bond-Driven Synergistically Enhanced Hyperpolarizability: Chiral Coordination Polymers with Nonpolar Structure Exhibiting Unusually Strong Second-Harmonic Generation. *Angew. Chem. Int. Ed.* **2021**, *60*, 20656–20660. [[CrossRef](#)]
13. Wu, K.; Yang, Z.; Pan, S. The first quaternary diamond-like semiconductor with 10-membered LiS<sub>4</sub> rings exhibiting excellent nonlinear optical performances. *Chem. Commun.* **2017**, *53*, 3010–3013. [[CrossRef](#)]
14. Abudurusuli, A.; Huang, J.; Wang, P.; Yang, Z.; Pan, S.; Li, J. Li<sub>4</sub>MgGe<sub>2</sub>S<sub>7</sub>: The First Alkali and Alkaline-Earth Diamond-Like Infrared Nonlinear Optical Material with Exceptional Large Band Gap. *Angew. Chem. Int. Ed.* **2021**. [[CrossRef](#)]
15. Lekse, J.W.; Moreau, M.A.; McNerny, K.L.; Yeon, J.; Halasyamani, S.; Aitken, J. Second-Harmonic Generation and Crystal Structure of the Diamond-like Semiconductors Li<sub>2</sub>CdGeS<sub>4</sub> and Li<sub>2</sub>CdSnS<sub>4</sub>. *Inorg. Chem.* **2009**, *48*, 7516–7518. [[CrossRef](#)]
16. Zhang, J.-H.; Clark, D.J.; Weiland, A.; Stoyko, S.S.; Kim, Y.S.; Jang, J.I.; Aitken, J.A. Li<sub>2</sub>CdGeSe<sub>4</sub> and Li<sub>2</sub>CdSnSe<sub>4</sub>: Biaxial Nonlinear Optical Materials with Strong Infrared Second-Order Responses and Laser-Induced Damage Thresholds Influenced by Photoluminescence. *Inorg. Chem. Front.* **2017**, *4*, 1472–1484. [[CrossRef](#)]
17. Zhang, J.-H.; Clark, D.J.; Brant, J.A.; Sinagra, C.W.; Kim, Y.S.; Jang, J.I.; Aitken, J.A. Infrared nonlinear optical properties of lithium-containing diamond-like semiconductors Li<sub>2</sub>ZnGeSe<sub>4</sub> and Li<sub>2</sub>ZnSnSe<sub>4</sub>. *Dalton Trans.* **2015**, *44*, 11212–11222. [[CrossRef](#)]
18. Ritscher, A.; Hoelzel, M.; Lerch, M. The order-disorder transition in Cu<sub>2</sub>ZnSnS<sub>4</sub>—A neutron scattering investigation. *J. Solid State Chem.* **2016**, *238*, 68–73. [[CrossRef](#)]
19. Liang, F.; Kang, L.; Lin, Z.; Wu, Y.; Chen, C. Analysis and prediction of mid-IR nonlinear optical metal sulfides with diamond-like structures. *Coord. Chem. Rev.* **2017**, *333*, 57–70. [[CrossRef](#)]
20. Kang, L.; Liang, F.; Jiang, X.; Lin, Z.; Chen, C. First-Principles Design and Simulations Promote the Development of Nonlinear Optical Crystals. *Accounts Chem. Res.* **2019**, *53*, 209–217. [[CrossRef](#)] [[PubMed](#)]
21. Chen, M.-M.; Xue, H.-G.; Guo, S.-P. Multinary metal chalcogenides with tetrahedral structures for second-order nonlinear optical, photocatalytic, and photovoltaic applications. *Coord. Chem. Rev.* **2018**, *368*, 115–133. [[CrossRef](#)]
22. Pauling, L. The principles determining the structure of complex ionic crystals. *J. Am. Chem. Soc.* **1929**, *51*, 1010–1026. [[CrossRef](#)]
23. Wu, H.; Zhang, B.; Yu, H.; Hu, Z.; Wang, J.; Wu, Y.; Halasyamani, P.S. Designing Silicates as Deep-UV Nonlinear Optical (NLO) Materials using Edge-Sharing Tetrahedra. *Angew. Chem. Int. Ed.* **2020**, *59*, 8922–8926. [[CrossRef](#)]
24. Zhang, J.-H.; Clark, D.J.; Brant, J.A.; Rosmus, K.A.; Grima, P.; Lekse, J.W.; Jang, J.I.; Aitken, J.A. α-Li<sub>2</sub>ZnGeS<sub>4</sub>: A Wide-Bandgap Diamond-like Semiconductor with Excellent Balance between Laser-Induced Damage Threshold and Second Harmonic Generation Response. *Chem. Mater.* **2020**, *32*, 8947–8955. [[CrossRef](#)]



25. Brant, J.A.; Clark, D.J.; Kim, Y.S.; Jang, J.I.; Zhang, J.-H.; Aitken, J.A.  $\text{Li}_2\text{CdGeS}_4$ , A Diamond-Like Semiconductor with Strong Second-Order Optical Nonlinearity in the Infrared and Exceptional Laser Damage Threshold. *Chem. Mater.* **2014**, *26*, 3045–3048. [[CrossRef](#)]
26. Li, G.; Chu, Y.; Zhou, Z. From  $\text{AgGaS}_2$  to  $\text{Li}_2\text{ZnSiS}_4$ : Realizing Impressive High Laser Damage Threshold Together with Large Second-Harmonic Generation Response. *Chem. Mater.* **2018**, *30*, 602–606. [[CrossRef](#)]
27. Rosmus, K.A.; Brant, J.A.; Wisneski, S.D.; Clark, D.J.; Kim, Y.S.; Jang, J.I.; Brunetta, C.D.; Zhang, J.-H.; Srncic, M.N.; Aitken, J.A. Optical Nonlinearity in  $\text{Cu}_2\text{CdSnS}_4$  and  $\alpha/\beta\text{-Cu}_2\text{ZnSiS}_4$ : Diamond-like Semiconductors with High Laser-Damage Thresholds. *Inorg. Chem.* **2014**, *53*, 7809–7811. [[CrossRef](#)]
28. Chen, J.; Chen, H.; Xu, F.; Cao, L.; Jiang, X.; Yang, S.; Sun, Y.; Zhao, X.; Lin, C.; Ye, N.  $\text{Mg}_2\text{In}_3\text{Si}_2\text{P}_7$ : A Quaternary Diamond-like Phosphide Infrared Nonlinear Optical Material Derived from  $\text{ZnGeP}_2$ . *J. Am. Chem. Soc.* **2021**, *143*, 10309–10316. [[CrossRef](#)]
29. SAINT, version 7.60A; Bruker Analytical X-ray Instruments Incorporated: Madison, WI, USA, 2008.
30. Spek, A.L. Single-crystal structure validation with the program PLATON. *J. Appl. Crystallogr.* **2003**, *36*, 7–13. [[CrossRef](#)]
31. Sheldrick, G.M. A short history of SHELX. *Acta Crystallogr. Sect. A Found. Crystallogr.* **2008**, *64*, 112–122. [[CrossRef](#)]
32. Mei, D.J.; Cao, W.Z.; Wang, N.Z.; Jiang, X.X.; Zhao, J.; Wang, W.K.; Dang, J.H.; Zhang, S.Y.; Wu, Y.D.; Rao, P.H.; et al. Breaking Through the “3.0 eV wall” of Energy Band Gap in Mid-Infrared Nonlinear Optical Rare Earth Chalcogenides by Charge-Transfer Engineering. *Mater. Horiz.* **2021**, *8*, 2330–2334. [[CrossRef](#)]
33. Jiang, J.Q.; Mei, D.J.; Gong, P.F.; Lin, Z.S.; Zhong, J.B.; Wu, Y.D. Wide Band Gap Design of New Chalcogenide Compounds:  $\text{KSrPS}_4$  and  $\text{CsBaAsS}_4$ . *RSC Adv.* **2017**, *7*, 38044–38051. [[CrossRef](#)]
34. Larson, A.C.; Dreele, R.B.V. *General Structure Analysis System (GSAS)*; Los Alamos National Laboratory, University of California: Oakland, CA, USA, 2004; pp. 86–748.
35. Kortüm, G. *Reflectance Spectroscopy*; Springer: Berlin, Germany, 1969.
36. Tauc, J. Absorption edge and internal electric fields in amorphous semiconductors. *Mater. Res. Bull.* **1970**, *5*, 721–729. [[CrossRef](#)]
37. Clark, S.; Segall, M.D.; Pickard, C.J.; Hasnip, P.J.; Probert, M.I.J.; Refson, K.; Payne, M.C. First principles methods using CASTEP. *Z. Krist.* **2005**, *220*, 567–570. [[CrossRef](#)]
38. Ceperley, D.; Alder, B.J. Ground State of the Electron Gas by a Stochastic Method. *Phys. Rev. Lett.* **1980**, *45*, 566–569. [[CrossRef](#)]
39. Perdew, J.P.; Zunger, A. Self-interaction correction to density-functional approximations for many-electron systems. *Phys. Rev. B* **1981**, *23*, 5048–5079. [[CrossRef](#)]
40. Perdew, J.P.; Wang, Y. Accurate and simple analytic representation of the electron-gas correlation energy. *Phys. Rev. B* **1992**, *45*, 13244–13249. [[CrossRef](#)]
41. Monkhorst, H.J.; Pack, J.D. Special points for Brillouin-zone integrations. *Phys. Rev. B* **1976**, *13*, 5188–5192. [[CrossRef](#)]
42. Bellaiche, L.; Vanderbilt, D. Virtual crystal approximation revisited: Application to dielectric and piezoelectric properties of perovskites. *Phys. Rev. B* **2000**, *61*, 7877–7882. [[CrossRef](#)]
43. Winkler, B.; Pickard, C.; Milman, V. Applicability of a quantum mechanical virtual crystal approximation’ to study Al/Si-disorder. *Chem. Phys. Lett.* **2002**, *362*, 266–270. [[CrossRef](#)]
44. Liu, B.W.; Zhang, M.J.; Zhao, Z.Y.; Zeng, H.Y.; Zheng, F.K.; Guo, G.C.; Huang, J.S. Synthesis, Structure, and Optical Properties of the Quaternary Diamond-Like Compounds  $\text{I}_2\text{-II-IV-VI}_4$  (I = Cu; II = Mg; IV = Si, Ge; VI = S, Se). *J. Solid State Chem.* **2013**, *204*, 251–256. [[CrossRef](#)]
45. Chen, J.; Hu, C.L.; Mao, F.F.; Zhang, X.H.; Yang, B.P.; Mao, J.G.  $\text{LiMg}(\text{IO}_3)_3$ : An Excellent SHG Material Designed by Single-Site Aliovalent Substitution. *Chem. Sci.* **2019**, *10*, 10870–10875. [[CrossRef](#)]
46. Wang, Z.; Zhang, M.; Pan, S.L.; Wang, Y.; Zhang, H.; Chen, Z.H.  $\text{Li}_{0.8}\text{Mg}_{2.1}\text{B}_2\text{O}_5\text{F}$ : The First Borate Fluoride with Magnesium-Oxygen-Fluorine Octahedral Chains. *Dalton Trans.* **2014**, *43*, 2828–2834. [[CrossRef](#)] [[PubMed](#)]
47. Abudurusuli, A.; Li, J.J.; Tong, T.H.; Yang, Z.H.; Pan, S.L.  $\text{LiBa}_4\text{Ga}_5\text{Q}_{12}$  (Q = S, Se): Noncentrosymmetric Metal Chalcogenides with a Cesium Chloride Topological Structure Displaying a Remarkable Laser Damage Threshold. *Inorg. Chem.* **2020**, *59*, 5674–5682. [[CrossRef](#)]
48. Abudurusuli, A.; Wu, K.; Pan, S.L. Four New Quaternary Chalcogenides  $\text{A}_2\text{Ba}_7\text{Sn}_4\text{Q}_{16}$  (A = Li, Na; Q = S, Se): Syntheses, Crystal Structures Determination, Nonlinear Optical Performances Investigation. *New J. Chem.* **2018**, *42*, 3350–3355. [[CrossRef](#)]
49. Wu, K.; Su, X.; Yang, Z.; Pan, S. An investigation of new infrared nonlinear optical material:  $\text{BaCdSnSe}_4$ , and three new related centrosymmetric compounds:  $\text{Ba}_2\text{SnSe}_4$ ,  $\text{Mg}_2\text{GeSe}_4$ , and  $\text{Ba}_2\text{Ge}_2\text{S}_6$ . *Dalton Trans.* **2015**, *44*, 19856–19864. [[CrossRef](#)] [[PubMed](#)]
50. Wu, K.; Pan, S.L.; Yang, Z.H.  $\text{Ba}_2\text{GeS}_4$  and  $\text{Mg}_2\text{SnS}_4$ : Synthesis, Structures, Optical Properties and Electronic Structures. *RSC Adv.* **2015**, *5*, 33646–33652. [[CrossRef](#)]